2D-2D and 2D-0D heterostructures of few layer phosphorene with transition metal chalcogenide (SnSe) and Organic molecules for optoelectronic applications

A thesis

submitted to

Indian Institute of Science Education and Research Pune

in partial fulfilment of the requirements for the

BS-MS Dual Degree Programme

by

Megha Suryakant Chougule

Indian Institute of Science Education and Research Pune

Dr. Homi Bhabha Road,

Pashan, Pune 411008, INDIA.

April, 2019

Supervisor: Prof. Satish Ogale

Certificate

This is to certify that this dissertation titled as "**2D-2D and 2D-0D heterostructures of few layer phosphorene with transition metal chalcogenide (SnSe) and Organics molecules for optoelectronic applications**" towards the partial fulfilment of the BS-MS dual degree programme at the Indian Institute of Science Education and Research, Pune represents study carried out by Megha S. Chougule at IISER, PUNE under the supervision of Prof. Satishchandra Ogale, Professor, Department of physics during the academic year 2018-2019.

Megha S. Chougule

Registration number: 20141174

Prof. Satishchandra Ogale

Supervisor

Committee:

Prof. Satishchandra Ogale (Supervisor)

Dr. Surjeet Singh (TAC)

Dedication

This thesis is dedicated to my family and all my friends, who have been constant source of support and encouragement.

Declaration

I hereby declare that the matter embodied in the report entitled **"2D-2D and 2D-0D heterostructures of few layer phosphorene with transition metal chalcogenide (SnSe) and Organics molecules for optoelectronic applications"** are the results of the work carried out by me at the Department of Physics, IISER PUNE, under the supervision of Prof. Satishchandra Ogale and the same has not been submitted elsewhere for any other degree.

Megha S. Chougule

Registration number: 20141174

Prof. Satishchandra Ogale

Supervisor

Acknowledgement

I would like to express my sincere gratitude to my thesis supervisor Prof. Satish Ogale for his guidance and constant support throughout my project work. Not only his valuable guidance, but also his never-ending encouragement was the key motivation in successful completion of this journey.

I would like to thank Dr. Padmini Pandey, Dr. Umesh Bansode, Dr. Subas Mudli and Dr. Channa Reddy for all the help and aid that they have provided throughout my project. It wouldn't have been possible to overcome many difficulties without their guidance.

I would also like to thank Dr. Atikur Rahman and Dr. Pramod Pillai for allowing me to use their lab facilities.

I am indebted to all the technical staff members Anil sir, Prashant sir , Yatish sir and all other staff members for making my research easier at IISER.

Further, I would like to express my gratitude to all the lab members for their suggestions and fruitful discussions. Special thanks to Dr. Vinila Bedeker and Swati for their constant support.

Last but not the least, none of this would have been possible without the support of my parents and my brother.

--- Megha

List of figures

List of abbreviations

2D: 2 Dimensional

BP: Black Phosphorous

FLBP: Few layer Black Phosphorous

XRD: X-ray Diffraction

TEM: Transmission electron Microscopy

SAED: Selected area electron diffraction

FESEM: Field emission scanning electron microscopy

NPs: Nanoparticles

EDAX: energy dispersive x-ray analysis

IR: Infra-red

NIR: Near infra-red

Abstract

Black phosphorous, a 2D semiconductor, has been intensively studied in the past few years because of its high electrical conductivity and anisotropic optical and thermal properties. Few layer black phosphorous has a tuneable band gap, which varies form 0.3 eV to 2 eV depending upon the number of layers present in the material. Due to these properties, black phosphorous has promising applications in the field of electronics and photovoltaics, however this research is still in its early stage. In this project, heterostructures of few layer black phosphorene (FLBP) were prepared with SnSe sheets, SnSe nanoparticles and highly fluorescent Aristolactum molecules. FLBP and SnSe are known to absorb in the NIR and IR regions. Extrapolating this information, BP-SnSe heterostructures were synthesised to check their possible applications as an NIR photodetector. Further, the Aristolactum molecules used in this project were found to be highly fluorescent and gave a strong absorbance in UV region. These molecules were thus combined with BP to form BP- organic molecule heterostructures. These heterostructures were studied for their possible application as a visible light photodetector.

Contents

1. Introduction

"There is plenty of room at the bottom"

— Richard P. Feynman

In 1959, Richard Feynman gave a talk at the annual meeting of the American Physical Society, where he talked about improving the technology by miniaturization and manipulation of materials at atomic scale. This lecture caught a lot of attention, and laid the conceptual basis of nanotechnology.[1] Today nanotechnology plays a major role in our everyday life. Nanomaterials are considered as a boon for electronics industry and medical science.[2] As a result, there is lot of ongoing research in these fields.

1.1. Two dimensional (2D) materials:

Materials which are confined to nanoscale in any dimension or have an internal structure on the nanoscale are called as nanomaterials.[3] 2D materials are the nanomaterials in which one dimension is confined to nanoscale. This One dimensional quantum confinement in 2D materials leads to the unique thermal, electrical and optical properties.[4] 2D materials provide the advantages such as light-weight, flexibility, multi-functionality etc. After the notable discovery of graphene, many other 2D materials like phosphorene, hexagonal boron nitride,

MXenes and transition metal dichalcogenides (TMDs) were intensively studied, and applied in the field of electronics and medicine.[5,6,7] People have developed 2D perovskite based solar cells, which has a photovoltaic efficiency of around 12.5%.[5] Recently, black phosphorous sheets were coupled with CRISPR-Cas9 (Clustered Regularly Interspaced Short Palindromic Repeats) system to enhance the release and delivery of CRISPR-Cas9 (genome editing tool) into cytosol of the cell.[8] Currently, people are trying to fabricate 2D semiconductors based transistors, as the major limitation posed by the usage of a silicon channel is the difficulty in obtaining a channel width below 5nm.[9] Making a channel below 5nm width in case of silicon devices leads to a drastic reduction in the electron mobility due to enhanced scattering.[10] While, on the other hand, in case of 2D semiconductors, due to vertical
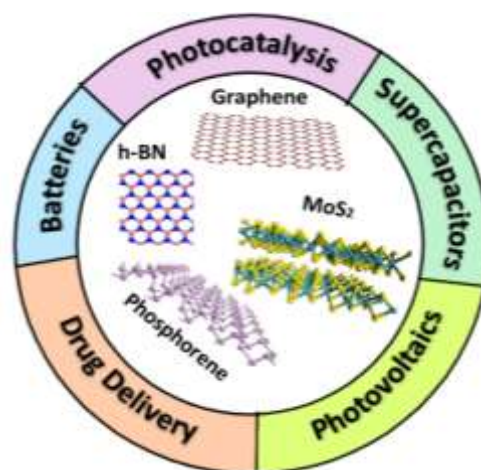
confinement there is a reduction in scattering. Thus, through very thin channels electron can move comparatively freely.[10] Thus, using a 2-D semiconductor gives an edge over due to the reduced size and enhanced efficiency. But this research is still at a preliminary stage.

1.2. Phosphorene:

2D Black phosphorous (phosphorene) is the most stable allotrope of phosphorous and it has an orthorhombic structure with Cmca space group, at room temperature.[11] BP is a layered material, which has strong intra-layer interaction (covalent in nature) and weak inter-layer interaction. This makes the exfoliation of thin layer feasible. Few layer phosphorene has a unique puckered structure which leads to strong in-plane anisotropy.[11] Hence, phosphorene has anisotropic optical, thermal and electrical properties, and this makes BP very unique.[12] The band gap of BP film varies from 0.3 eV (bulk) to 2 eV (monolayer) depending upon the number of layers present in the film.[13] Thus, by changing thickness of BP, the band gap of heterostructure with phosphorene can be easily tuned. Moreover, black phosphorous has a high electrical conductivity.[14] However, BP is very unstable in air due to the lone pair of electrons being oriented out of the plane. This is one of the major drawbacks due to which applications of BP are limited.
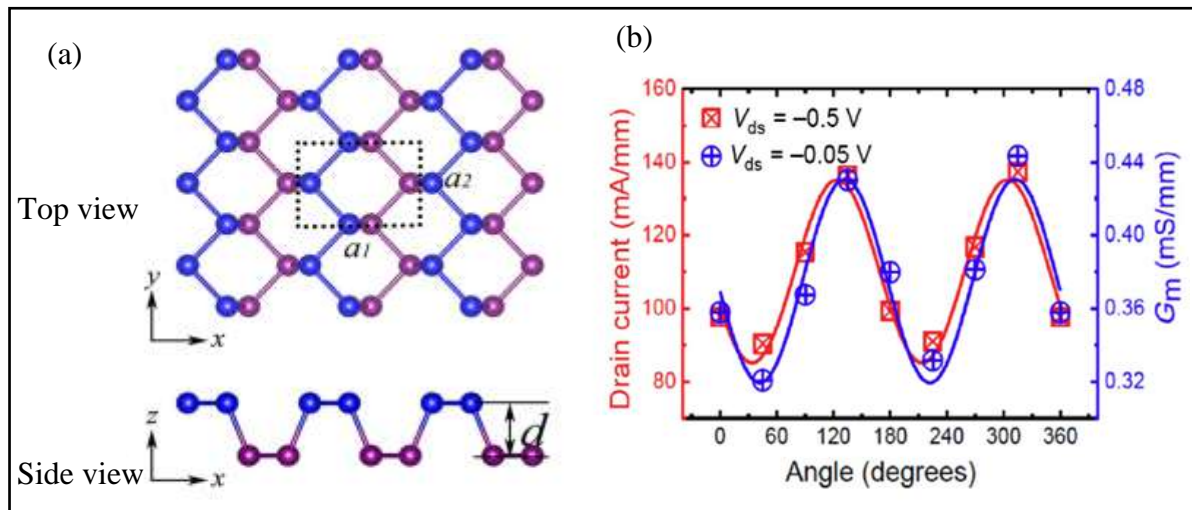
Figure 1: (a) Schematic structure of Single layer phosphorene [15] (b) Drain current measured at different angle (contacts, 45° apart from each other were used for the angle dependent measurement)[16]

Figure 1a shows the top view and side view of the single layer of BP with pucker height d. Pucker width in BP is 0.21nm. Angular dependence of drain current can be seen in Figure 1b, which relates to the anisotropic electrical properties.

1.3. Tin Selenide (SnSe):

SnSe is an anisotropic and robust, layered material.[17] It is isoelectric and has puckered structure like BP.[17] At room temperature it exists in orthorhombic phase with Pnma space group.[18] The most interesting fact about SnSe is that even though it has a high electrical conductivity its thermal conductivity is extremely low.[19] Hence, SnSe is one of the promising candidate for thermoelectric applications. Recently, people have realized Markov chain algorithm in SnSe based device, due to which a single device could do the work of 13,700 transistors.[30]
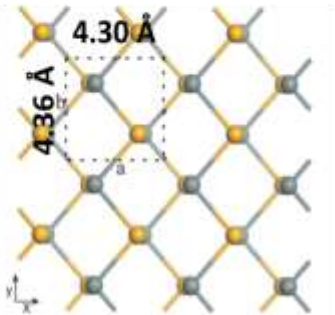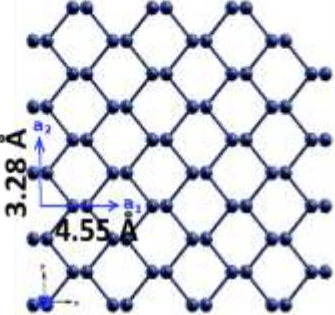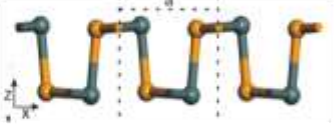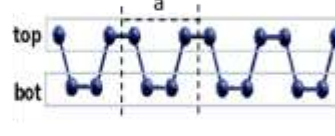
	SnSe	Phosphorene
Top view		
Side view from armchair direction		
Direct Band Gap	1.1 eV (bulk), 1.44 eV (monolayer)	0.3 eV (bulk), 2.1 eV(monolayer)
Carrier Mobility at 300K	$10000 \ cm^2V^{-1}S^{-1}$ (Monolayer)	$1000 \ cm^2V^{-1}S^{-1}$ (10 nm thickness)
Thermal conductivity at 300K	$< 3 \ W \ m^{-1}K^{-1}$ (Monolayer)	11.77 to 17.42 $W \ m^{-1}K^{-1}$ (9.5 nm thick)

Table 1: Comparison of BP and SnSe [20,21,22,23,24]

As depicted in table 1, SnSe is more symmetric and has higher carrier mobility than BP. Also SnSe has good stability in air. But its applications are limited because of fragile nature and difficulty in maintaining the high ZT value at temperatures lower than 650°C.

1.4. Heterostructures based on 2D materials:

Composite structures which consists of two or more layers of different materials are referred as Heterostructures. They manifest extraordinary properties that may not exist in individual materials.[23] Combining two different structures may lead to redistribution of charges, and structural changes. These changes can be further handled by changing the external parameters and orientation of the individual components.[31] 2D materials provide great platform for designing heterostructures with diverse properties. E.g. Effects like Charge density waves (CDW) and spin density waves (SDW) can be induced in crystals with transition metal sandwiched between 2D materials.[31] Further, within these heterostructures, there is a class of mixed dimensional van der Waals heterostructures which are even more fascinating. In case of mixed dimensional heterostructures, as lattice matching is not beholden, the interface is more complex and less constrained.[25] Hence mixed dimensional heterostructures can be more flexible.

Thus, this project is aimed at exploring and understanding the characteristics of the 2D-2D heterostructures and mixed dimensional heterostructures and extrapolating these studies to construct a photovoltaic device. To achieve this aim, 2D-2D and 2D-0D heterostructures of few layer black phosphorous (FLBP) were synthesised by combining BP with SnSe and organic molecule. SnSe has high carrier mobility and good stability in air at room temperature, hence an attempt was made to couple the properties of BP and SnSe to increase the stability of BP and make an efficient material for optoelectronic applications. Furthermore, both BP and SnSe are highly anisotropic and can absorb in NIR and IR regions. Thus there is a possibility of BP-SnSe heterostructure being a polarization sensitive NIR/IR photodetector. Moreover, BP-organic molecule heterostructures were explored to check its possible applications in building a visible-light photodetector.

2. Experimental methods:

2.1. Materials

Black phosphorus crystal pieces (purchased from smart elements, GmbH), Tin Selenide crystals, Aristolactum molecules, L-ascorbic acid, Sodium borohydride, Se powder, anhydrous tin chloride, indium tin oxide (ITO) coated Polyethylene Terephthalate (PET).

Solvents: anhydrous N-Methyl-2-Pyrrolidone (NMP), anhydrous toluene, Tetrahydrofuran (THF)

Except BP, SnSe crystals and Aristolactum molecules all other chemicals were purchased from Sigma Aldrich.

2.2. General Characterizations

(I) XRD:

Powder X-ray diffraction (PXRD) pattern is one of the powerful technique used for structural analysis, phase identification and quantification of the material. PXRD data were collected at a tube voltage of 40 kV and a tube current of 30 mA using a Bruker D8 Advance X-ray Diffractometer with Cu k-α radiation (λ=1.5417Å) Step size, scan speed, rotation and other parameters were varied and optimized for each sample.

(II) FESEM and EDAX:

Zeiss Ultra plus Field emission scanning electron microscope (FESEM) equipped with energy dispersive x-ray analysis (EDAX) was used to understand topographic details and composition of the samples. The FESEM images were recorded at a 3kV operating voltage. For SEM all the samples were prepared on silicon substrate and then placed on carbon tape for imaging. EDAX was also done during FESEM.

(III) Raman Spectroscopy:

Intensity and frequency of the peaks in Raman spectra are very unique for each material. Raman spectroscopy is used for identifying unknown material, understanding interlayer interactions, changes in the crystallinity etc. For Raman spectroscopy, samples were prepared on silicon substrate and stored in vacuum. Raman data of the samples were collected using RENISHAW spectrometer equipped with diode laser of 532nm in backscattering geometry. The power of the laser is 17 mW. Backscattering geometry was preferred to get better spatial resolution. A synapse charge coupled device was used as detector.

(IV) TEM-HRTEM:

Transmission electron microscopy (TEM) is a technique used for compositional, morphological and crystallographic analysis. TEM works on the same basic principles as optical microscope. In TEM, high energy electrons produced using field emission gun are shined onto the sample to get image. HRTEM is a special mode of imaging in TEM, which uses both the scattered and the transmitted electrons to create an image. We have recorded the TEM data using JEM 2200FS TEM, which has 200 KeV field emission gun. Also it is equipped with EDS-Oxford X-MAX N 100 TLE and HAADF detector. HAADF detector is used in elemental mapping. For TEM, dilute solutions of the samples were prepared in toluene and drop-casted on a copper grid coated with ultrathin carbon. These samples were then dried under sodium lamp for 10 minutes.

(v) Optoelectronic measurements:

Optoelectronic measurements of BP-SnSe devices were done using Keithely 2420. We have used solar simulator and IR lamp for doing measurements. IR lamp spectra ranges from 780nm to 1400 nm with maxima around 830nm. IR lamp heats the sample, so to minimize thermoelectric effect sample was kept at a distance of 20-25cm from the source. FLBP-organic molecule heterostructures devices were tested using 405 nm laser (<50mW) and LED (9 mW).

2.3. Synthesis

(A) BP-SnSe (2D-2D) Heterostructure:

BP-SnSe composite was synthesized by exfoliating BP and SnSe together in NMP (1 methyl-2pyrrolidione) using ultrasonic Probe Sonicator. Equal numbers of moles of BP and SnSe were mixed with the help of mortar pestle in glove box. Then the mixture was transferred to a bottle and around 80-100 ml of NMP was added to it. Sample was sonicated for 6 hours with 5sec on and 5 sec off time by using Probe Sonicator. The bottle was placed in ice bath while doing sonication to maintain optimal temperature. After 6 hours of sonication, 80% of the supernatant was centrifuged at 1000 rpm for 1hour in centrifuge tube. Now 80% of the supernatant of centrifuged solution was transferred to another tube and centrifuged at 6000 rpm for an hour. The residue (which we got after 2nd centrifugation) was collected in a glass vial and stored at room temperature. This residue contained the exfoliated BP-SnSe. For reference, BP and SnSe crystals were also exfoliated separately in NMP using Probe Sonicator.

(B) SnSe nanoparticles:

SnSe nanoparticles (NPs) were synthesized by co-precipitation method as reported by B. Pejjai et al.[26] 1 mmol of anhydrous $SnCl_2$ and 10 mmol of L-ascorbic acid were added to 25 ml of DI water. The solution was stirred at 70°C in the ambient atmosphere till we get a clear solution. The clear solution indicates the formation of $H_2Asc\text{-}Sn^{2+}$ ion complexes. Besides, 0.9 mmol of Se-powder was dissolved in 25 ml of DI water in presence of 1.2 mmol of $NaBH_4$. This solution was stirred at 70°C for 10 min and added to the solution containing $H_2Asc\text{-}Sn^{2+}$ ion complexes. Next, the final mixture was heated at 90°C for 10-12 min and allowed to cool at room temperature. After cooling, the reaction mixture was centrifuged at 6000 rpm for 10 min and a black precipitate was obtained.
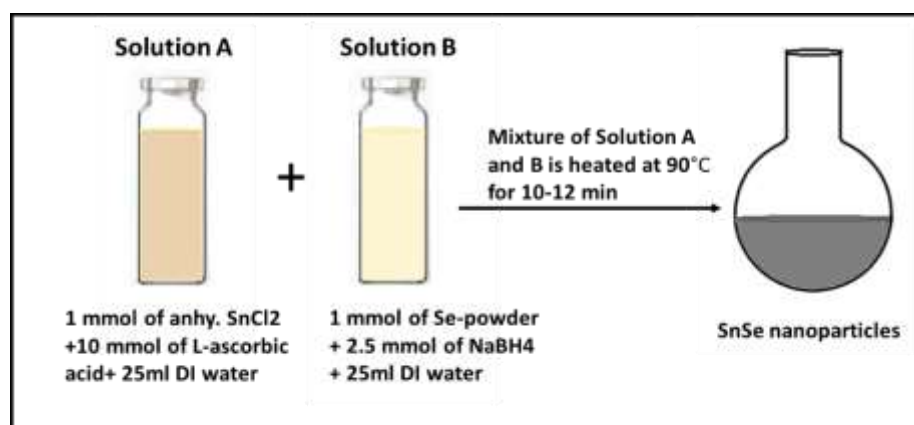

Figure 2: Schematic representation of synthesis procedure of SnSe nanoparticles

(C) FLBP-SnSe NPs (2D-0D) heterostructure:

FLBP-SnSe NPs heterostructures were synthesised by adding equal moles of BP and SnSe nanoparticles and stirring this reaction mixture for 5 hrs at room temperature. This reaction mixture was then further sonicated for about 30 minutes to enhance the interaction between BP and SnSe NPs. This sample was then characterised further using XRD, UV spectroscopy, SEM and TEM techniques to study the heterostructure. Also, photo-voltaic measurements were done to check the possible applications of the sample in photodetectors.

(D) BP-Organic molecules (2D-0D) Heterostructure:

In order to prepare BP-Organic molecule heterostructure, BP was exfoliated following the same protocol as mentioned earlier. Further, three Aristolactum molecules (CH-481, CH-494 and CH-549, refer Appendix) which were potentially suitable to make these heterostructures were

chosen. A stock solution (8 x 10^{-4} M) was prepared for each compound using THF of spectroscopic grade. PL measurements were then done for these solutions for which 3 ml solutions of concentration 8 x 10^{-6} M were prepared in glass vials by adding NMP to 30 µl of stock solution. Aristolactum+BP solution sample was prepared by adding 350 µl of exfoliated BP (1.22mg/ml) and 2.65 ml of NMP to 30 µl of stock solution of Aristolactum. BP+Aristolactum solution is sonicated well.
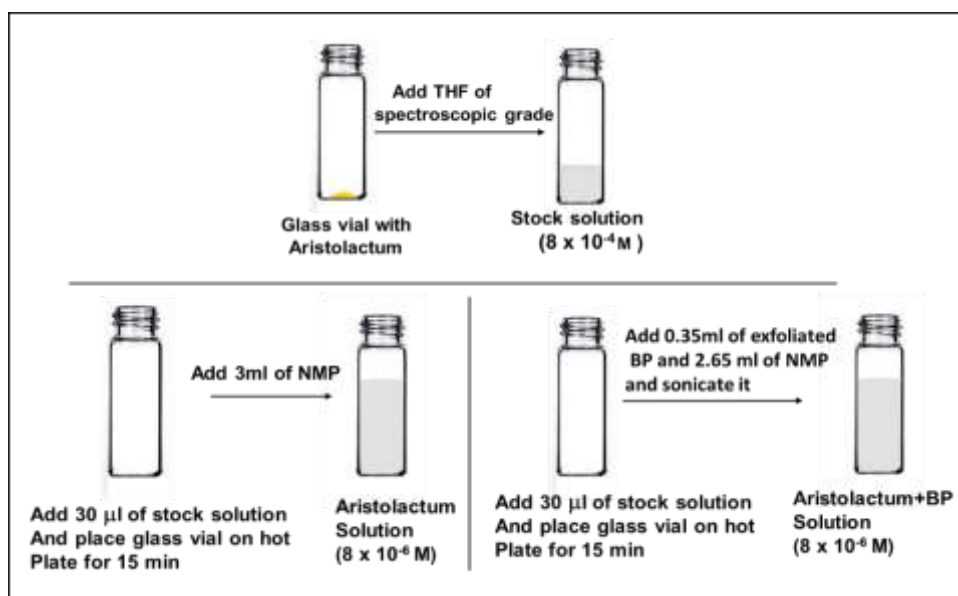
Figure 3: Schematic representation of the procedure followed to prepare BP-organic molecules heterostructure

2.4. Fabrication of primitive photovoltaic device

For the device fabrication we used a 1.5 cm x 2.0 cm ITO coated PET sheet as a substrate. First, channel was made by scratching the conducting side with the help of a surgical blade. The channel length was around 80-100□m. Then we drop casted the sample at the centre of the channel (Figure 4).

Figure 4: Schematic representation of the device

3. Results and discussion:

3.1. BP-SnSe (2D-2D) heterostructure:

3.1.1. XRD

To confirm the formation of the BP-SnSe heterostructure, structural analysis of the samples was done on glass substrate at room temperature. Figure 5 shows the X-ray diffraction patterns of FL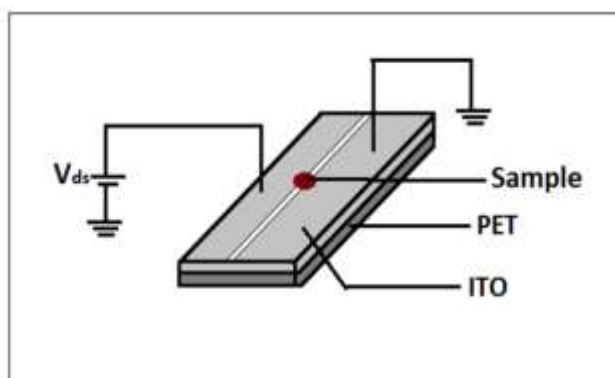BP, SnSe sheets and BP-SnSe (2D-2D) heterostructure. XRD pattern of liquid-exfoliated BP shows three peaks for (020), (040) and (060) crystal planes at 2-theta values of 16.91°, 34.21° and 54.43° respectively, while XRD pattern of SnSe sheets shows a single peak corresponding to (400) plane at 31.03° 2-theta value. Hump seen in the XRD pattern of FLBP corresponds to glass. In case of heterostructure, peaks corresponding to (020) and (040) planes of BP and (400) plane of SnSe can be seen. This confirms the presence of both black phosphorous and SnSe in the heterostructure. We can see that there is decrease in intensity and slight broadening of XRD peaks of the heterostructure. Strain in the heterostructure is one of the factor responsible for the broadening, however interface roughness and induced defects might led to the broadening as well .[42]
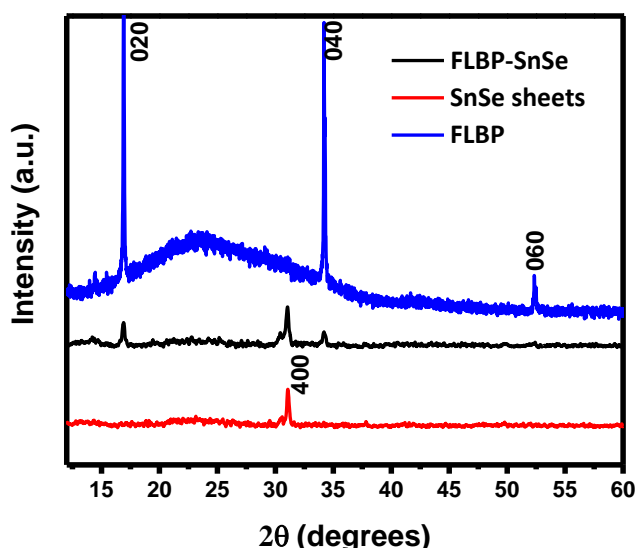
Figure 5: XRD pattern of BP-SnSe (black line), FLBP (blue line) and SnSe sheets (red line). XRD of BP-SnSe composite confirms the presence of both few layer phosphorene and SnSe

3.1.2. UV-VIS-NIR Spectroscopy

UV-Vis-NIR absorption spectra of FLBP, SnSe and BP-SnSe (2D-2D) heterostructure were studied to determine the optical band gap (Figure 6a). All the three samples shows broad absorption band covering the entire UV-Vis-NIR region. Both scattering and absorption are contributing to the absorption spectra. In Figure 6a, it can be seen that absorbance of the BP-

SnSe heterostructure in the 300 nm to 600 nm range was less than FLBP and SnSe sheets, while absorbance of the heterostructure was more in the 800 nm to 1300 nm range as compared to FLBP and SnSe sheets. We have calculated the optical band gaps of FLBP, SnSe and BP-SnSe using the Tauc relation, which is given by equation (1).

$$\alpha h\upsilon = A\,(h\upsilon - E_g)^n \quad \text{———— (1)} \qquad (n = 0.5 \text{ for direct allowed transition})$$

The estimated direct Optical band gaps (from Tauc plots) of FLBP and SnSe sheets are 1.7 eV and 1.1 eV respectively (Figure 6b and c). In case of FLBP, the estimated value is consistent the reported value of direct optical band gap for phosphorene (monolayer or bilayer BP).[37, 38] But the exact thickness of FLBP needs to be measured using AFM. In case of SnSe sheets, estimated direct optical band gap matches with the reported value.[39,40] The thickness of the SnSe sheets might be 30 nm ± 10 nm.[39, 40]
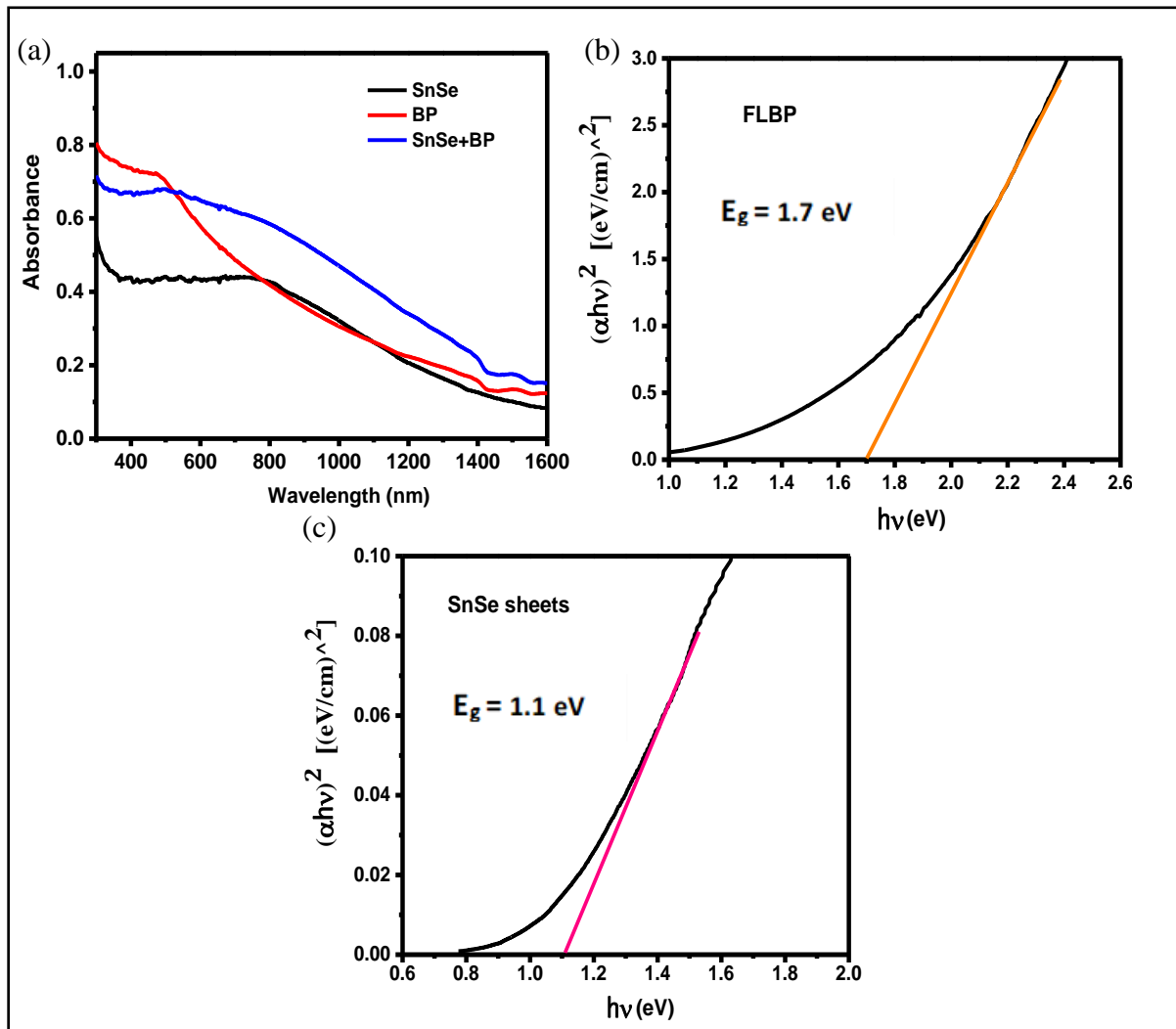

Figure 6: (a) UV-Vis-NIR absorbance spectra of FLBP (red line), SnSe sheets (black line) and BP-SnSe heterostructure (blue line). (b) and (c) are Tauc plots of FLBP and SnSe sheets.

3.1.3. Raman spectroscopy

FLBP, SnSe sheets and BP-SnSe (2D-2D) composite were characterized by using Raman spectroscopy on p-type silicon substrate at 10% power (1.7mW) using 532 nm laser to confirm the formation of BP-SnSe heterostructure, and to get information concerning structure, phase of the heterostructure and interlayer interaction. In the Raman spectra of black phosphorous (Figure 7a and b), peaks at 361.4 cm^{-1}, 437.8 cm^{-1} and 466.2 cm^{-1} corresponding to A^1_g (in plane), B_{2g} (out of plane) and A^2_g (out of plane) phonon modes can be seen. These Raman peaks confirms that black phosphorous used in this work is orthorhombic. In the Raman spectra of BP-SnSe heterostructure, characteristic Raman peaks of both black phosphorous and SnSe can be seen. The Peak observed at 520.2cm^{-1} in Raman spectra of all the samples corresponds to silicon. Raman peaks at 358.6 $cm^{-1,}$ 434.6 cm^{-1} and 462.4 cm^{-1} in BP-SnSe heterostructure are attributed to corresponding A^1_g, B_{2g} and A^2_g phonon modes in orthorhombic black phosphorous. We can clearly see that Raman peaks of BP in BP-SnSe are shifted towards left (Figure 7b). The shift in Raman peaks towards lower wavenumber suggests that there is interaction between BP and SnSe sheets. Most likely the interaction between BP and SnSe is van der Waals interaction, which can be confirmed by using few other characterizations. In Figure 6b, we can see that there is broadening in the Raman peaks of heterostructure. The cause of this might be the relative increase in disorder.[36]

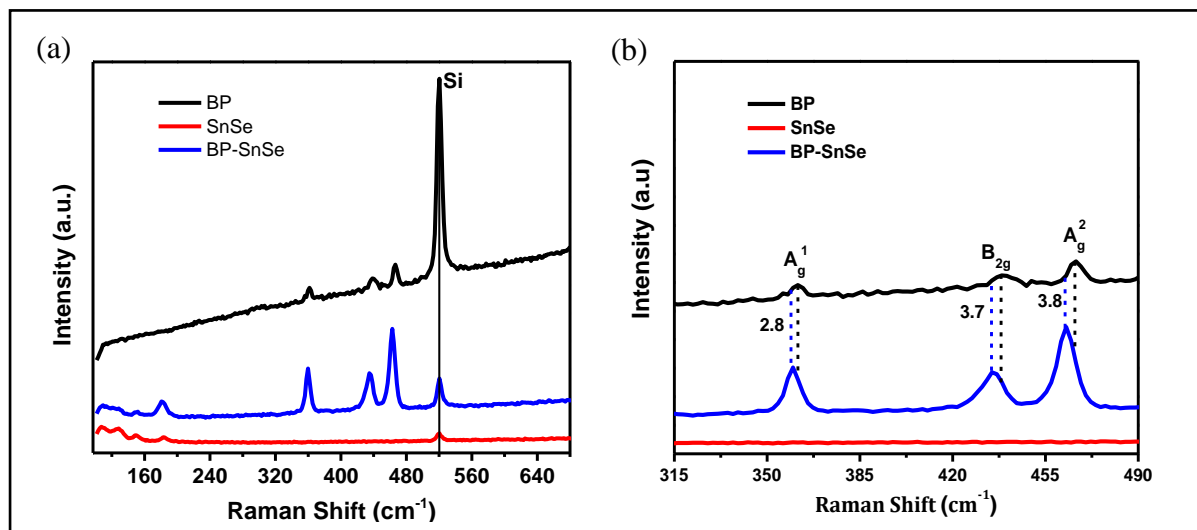Figure 7: (a) Raman Spectra of BP (black line), BP-SnSe (blue line) and SnSe (red line) on p-type silicon substrate at 10mW electrical power. Raman spectra of the BP-SnSe (blue line) confirms the presence of both BP and SnSe. (b) Enlarged Raman spectra of the samples. A^1_g, B_{2g} and A^2_g modes in the Raman spectrum belongs to phosphorene and shift in the peaks allude to the interaction between BP and SnSe.

3.1.4. SEM and EDAX

To understand the surface morphology and composition of the heterostructure Scanning electron microscopy (SEM) was done. Figure 8a, b shows SEM images of BP-SnSe heterostructure deposited on silicon substrate. We can see the layered sheets of BP-SnSe in SEM images. Figure 8c shows Energy Dispersive X-ray Analysis (EDAX) spectra of the sample, which has peaks corresponding to P, Sn and Se. This confirms the presence of both BP and SnSe.

Element	Weight %	At. %
P	41.04	68.93
Sn	33.68	15.60
Se	45.29	15.47
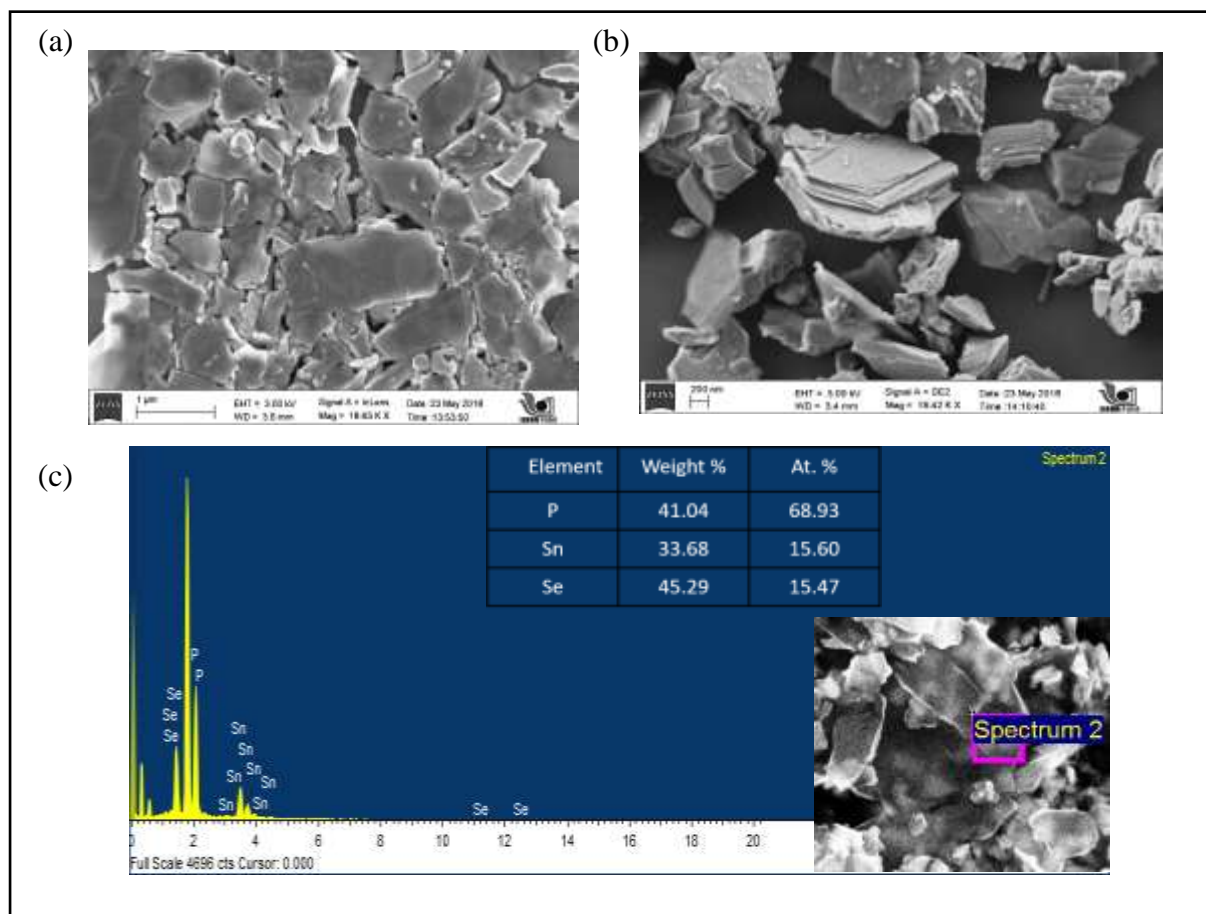
Figure 8: (a, b) SEM images of BP-SnSe heterostructure. (c) EDAX of the heterostructure confirming the presence of both BP and SnSe

3.1.5 Photocurrent Measurements

I-V characteristics of the measured dark current and photocurrent are shown in Figure 9. In case of FLBP, small deviation from ohmic behaviour can be seen (Figure 9a and b). FLBP shows no change in the current under visible light illumination, while change observed under NIR light illumination was very small. This can be ascribed to low absorption coefficient of the BP.[32]

Figure 9: (a, b, c) light I-V characteristics of FLBP and SnSe sheets in the dark and under illumination. (d, e) I-V characteristi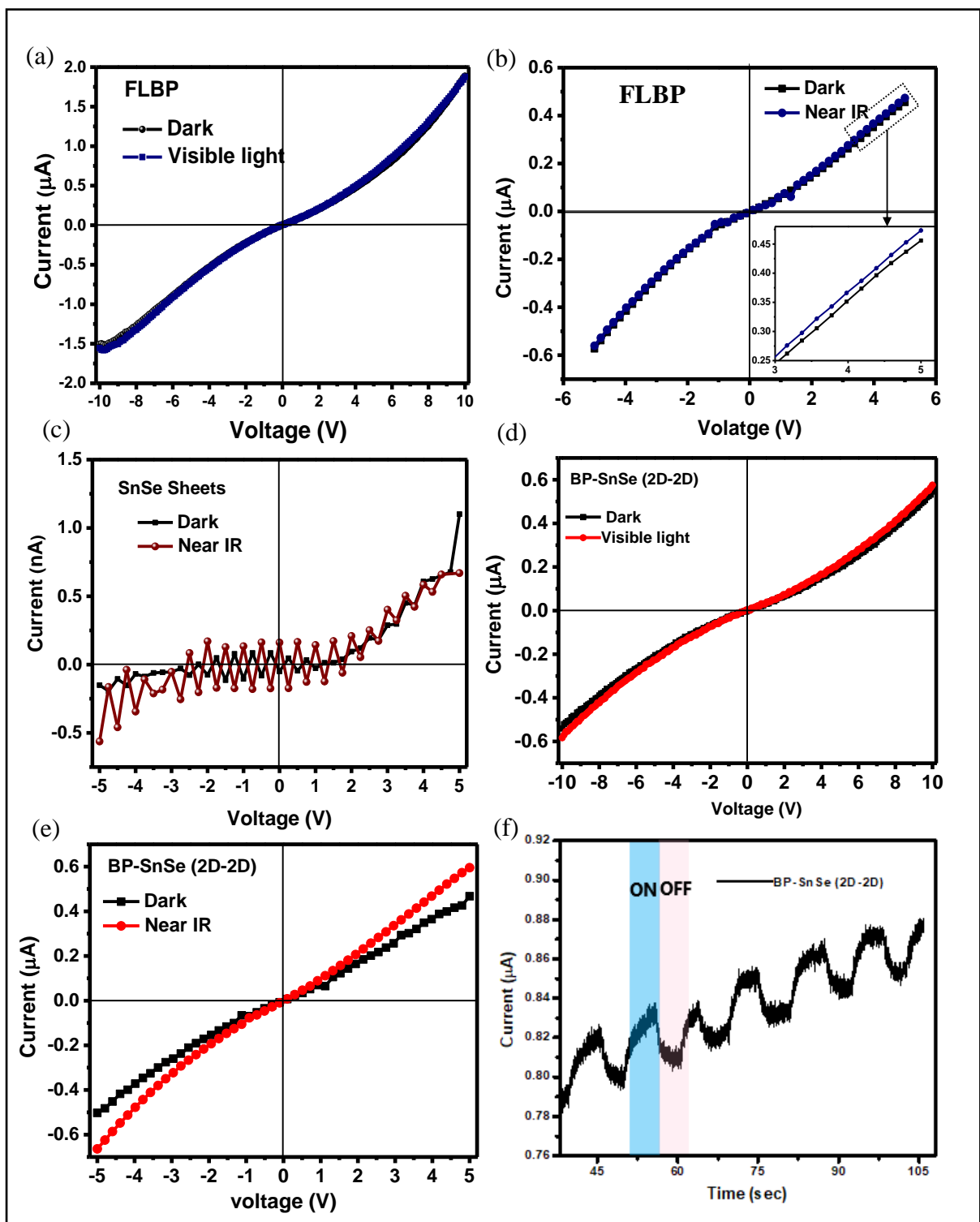cs of BP-SnSe (2D-2D) heterostructure in the dark and under illumination with visible and NIR (f) The current-time curve of the device with BP-SnSe heterostructure at a 10V bias under NIR light illumination. Here ON (OFF) denotes illumination is ON (OFF).

In case of SnSe sheets, I-V characteristics of the current recorded in the dark and under illumination were asymmetric.(figure 9c). SnSe also didn't show any significant change in current under illumination. Figure 9d,and e shows the I-V characteristics of BP-SnSe (2D-2D) heterostructure. Under visible light illumination BP-SnSe heterostructure shows negligible change in the current. While, a change in the current under NIR light illumination can be clearly noticed in this case. One of the reasons for the enhancement in the current is BP-SnSe heterostructure absorbs more in near IR region as compared to FLBP and SnSe (Figure 5a). Optical band gap also suggests that the heterostructure can absorb effectively in NIR region (1240/1.31 = 946.5 nm). Time resolved photo-response of the device was investigated at room temperature under NIR illumination at 5V bias (Figure 9f). In the study of temporal photo-response of BP-SnSe, it was observed that current increases (decreases) when we switched ON (OFF) the light source and reaches a saturation. However, the maxima of the current upon illumination increased every time on switching ON the light source. The plausible reason behind this might be the accumulation of the charges in the conduction band. However, the exact reason has to be figured out by further investigation.

3.2. SnSe Nanoparticles:

3.2.1 XRD

The XRD pattern of the synthesized SnSe NPs deposited on glass substrate is shown in Figure 10, which matches with the XRD pattern of the orthorhombic Tin Selenide (JCPDS 03-065-3767).
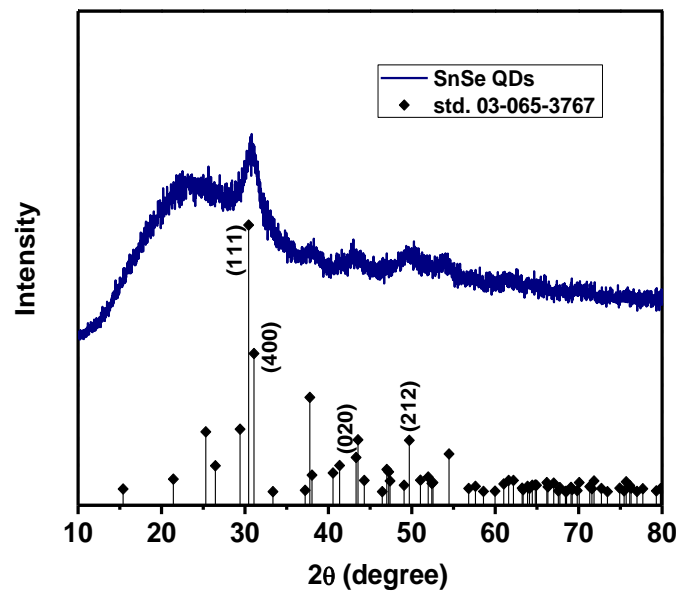

Figure 10: XRD pattern of SnSe nanoparticles on glass substrate at room temperature, which matches with the JCPDS 03-065-3767.

In Figure 10, we can see that XRD peaks are broad with dominant (111) orientation. Because of broadening, peaks that are very close to each other look like they are almost merged. For example, peak corresponding to (400) plane is almost merged with the peak corresponding to (111) plane. The broadening of the XRD peaks is mainly because of small particle size. Another factor that might be contributing in broadening of peaks is anisotropic particle shape. Peak width is inversely proportional to particle size and cosθ.[41] Hence peak broadening is more pronounced at larger values of 2θ. And the hump in the XRD pattern is because of glass substrate. By using equation (2) and (3) we calculated the lattice parameters from XRD pattern. 2θ values corresponding to (400), (020) and (111) planes are used for calculation. a = 1.15 nm, b = 0.415 nm and c = 0.444 nm are the calculated lattice constants which are consistent with the reported values.[28]

$$\lambda = 2d\sin\theta \qquad\text{———} \qquad (2)$$

$$\frac{1}{d^2_{hkl}} = \frac{h^2}{a^2} + \frac{k^2}{b^2} + \frac{l^2}{c^2} \qquad\text{———}\qquad (3)$$

3.2.3. EDAX

Compositional analysis of the sample was done using EDAX system on the SEM. To get more precise ratio of Sn:Se, EDAX was done randomly in four regions (Table 2). Molar ratio of Sn:Se used in the reaction was 1.11. Average Atomic% (At %) ratio Sn:Se is 1.16, which is nearly stochiometric.
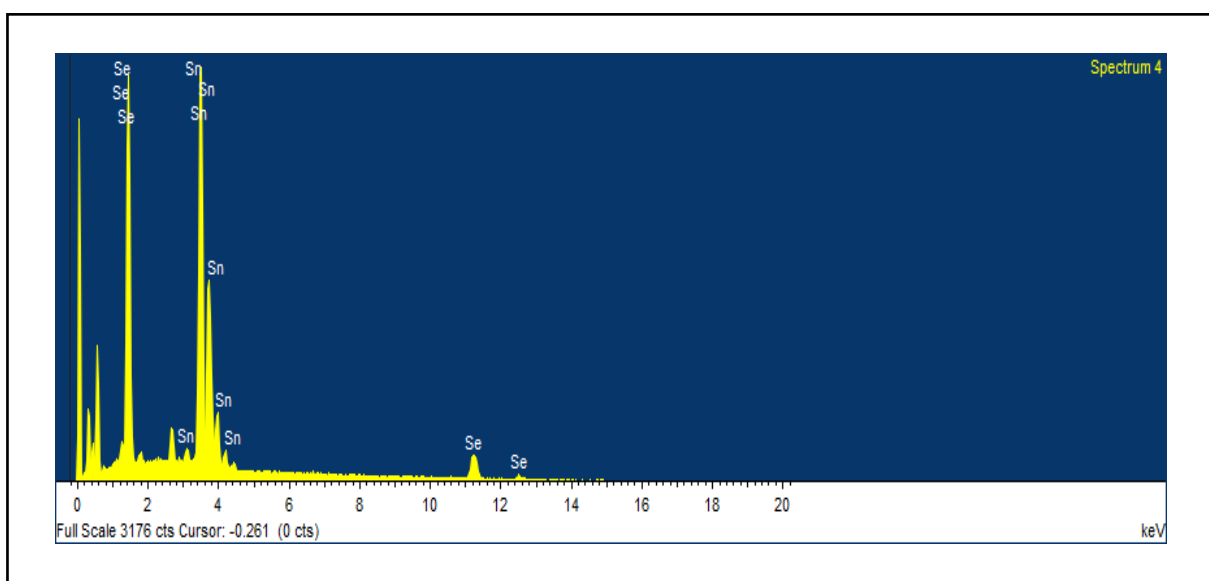

Figure 11: EDAX data of the synthesized SnSe nanoparticles. Inset image shows the analysed region

Spectrum	1	2	3	4
At % of Sn	54.19	53.10	52.25	54.08
At% of Se	45.81	45.92	45.75	45.93
ratio	1.18	1.15	1.14	1.17

Table 2: Elemental composition and ratio of Sn:Se

3.2.2 TEM

Transmission electron microscopy (TEM) image of SnSe nanoparticles (shown in Figure 12a) alludes that most of the nanoparticles possess round shape. Analysis of TEM images revealed
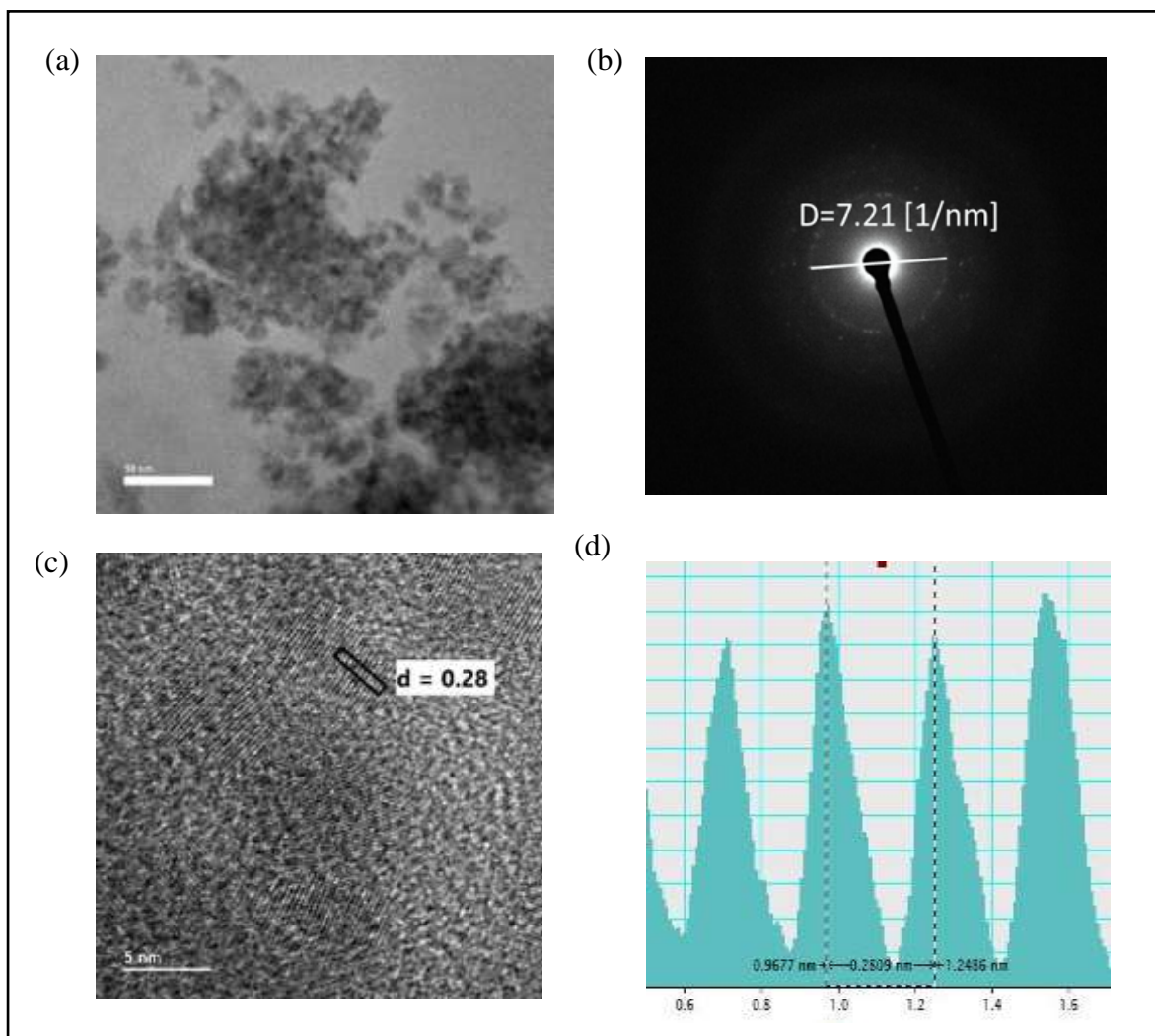

Figure 12: (a) TEM image of SnSe nanoparticles. Size of nanoparticles is in the range of 8nm to 10nm. (b) Selected area electron diffraction pattern (SAED) of SnSe nanoparticles. SAED pattern (small spots with continuous Debye rings) indicates poly-nanocrystalline nature of the sample. (c) HRTEM image of SnSe NPs. (d) Analysis of HRTEM image using digital micrograph software from gutan.

that size of nanoparticles varies from 8 nm to 12 nm. Analysis of High resolved TEM (HRTEM) image (Figure 12c) suggests that interlayer spacing is 0.28 nm and NPs are oriented along (111) plane. In SAED pattern (analysed using CrysTbox software), dim spots with light continuous rings can be seen, which indicates that the SnSe nanoparticles (d = 0.277 nm) are poly-nanocrystalline in nature (Figure 12b). The d-spacing was calculated using equation (4)

$$d = 1/2D \qquad \text{————} \qquad (4) \qquad \text{(d:-d-spacing, D: - diameter of the first ring)}$$

3.3. FLBP-SnSe NPs (2D-0D) heterostructure

3.3.1 XRD

Figure 13a shows the XRD pattern of FLBP, SnSe nanoparticles and FLBP-SnSe NPs (2D-0D) heterostructure. In the XRD pattern of BP-SnSe heterostructure, we can see the peaks of both FLBP and SnSe NPs. XRD Peaks in the case of FLBP-SnSe NPs heterostructure are relatively broader because there is more anisotropy in the shape of components present. Peaks of corresponding to BP for planes (020) and (040) can be clearly seen in Figure 13b at 2θ values of 16.92°, 34.28°. And peak corresponding to (111) plane of SnSe is at 29.45° which is shifted by 0.25° to the left. The shift in the XRD alludes to the strain in the heterostructure.[35]
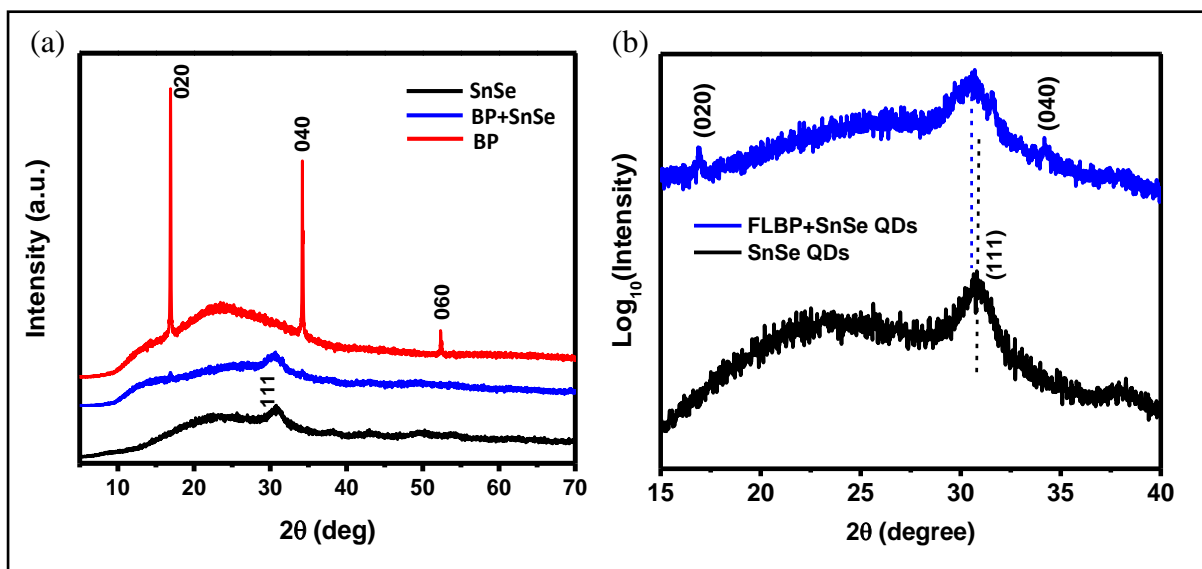

Figure 13: (a) XRD pattern of BP (red line), SnSe nanoparticles (black line) and BP-SnSe nanoparticles heterostructure (blue line). (b) XRD of BP and BP-SnSe on log_{10} scale.

3.3.2. SEM and EDAX

Analysis of surface morphology and composition of the prepared heterostructure was done using SEM and EDAX. Figure 14a, shows the SEM image of FLBP-SnSe (2D-0D) heterostructure. The EDAX data (Figure 13c) confirms the presence of both BP and SnSe. The EDAX analysis shows that the atomic% ratio Sn:Se is 1.04, in good agreement with the stoichiometry. As SnSe NPs are small in size and have a tendency to form small clumps, they can't be clearly seen from SEM image. Nanoparticles were not very uniformly distributed on BP-sheets and the same can be observed in the EDAX data (Figure 14c) as well as electron image (Figure 14b). The atomic % of BP is less as compared to SnSe because of the formation of SnSe clumps.

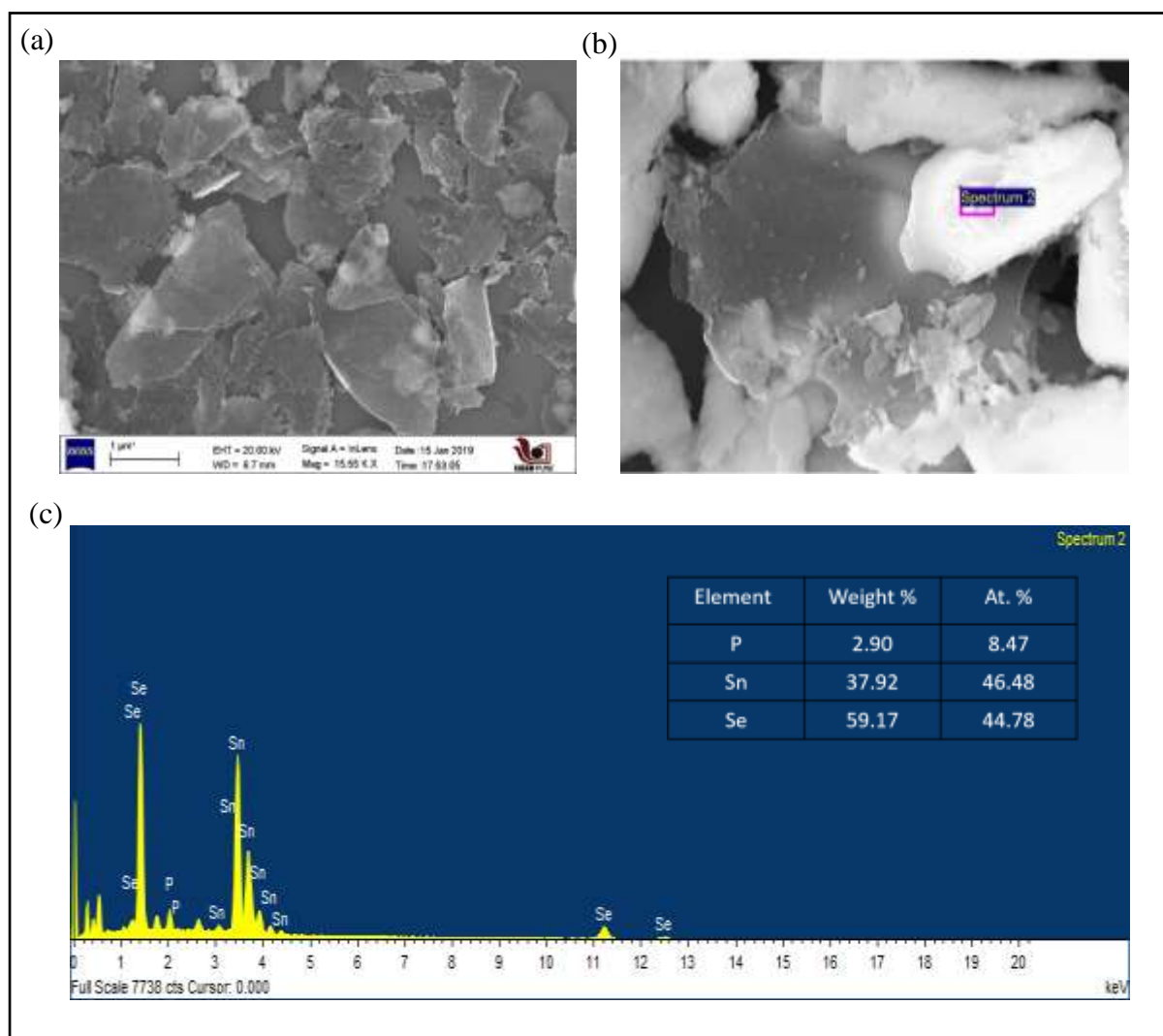| Element	Weight %	At. %
P	2.90	8.47
Sn	37.92	46.48
Se	59.17	44.78

Figure 14: (a) SEM image of BP-SnSe nanoparticles composite (b) Electron image showing the region on which EDAX was done (c) EDAX of FLBP-SnSe (2D-0D) heterostructure.

18

3.3.3. Raman Spectroscopy

Interaction between FLBP and SnSe NPs was investigated using Raman spectroscopy. Raman spectroscopy of BP and FLBP-SnSe NPs was done on silicon substrate using 532nm laser at 10% power i.e. 1.7 mW (Figure 15a). Peaks observed at 357.8cm^{-1},460 cm^{-1} and 432.2cm^{-1} are attributed to corresponding A^1_g, A^2_g and B_{2g} phonon modes of BP. In Figure 15b, red shift in Raman peaks can be distinctly seen, which stipulate the strain induced in heterostructure.[34] This is an evidence for the interaction between BP sheets and SnSe nanoparticles. Moreover, we can also see the broadening in peaks because of relative increase in disorder.[36]
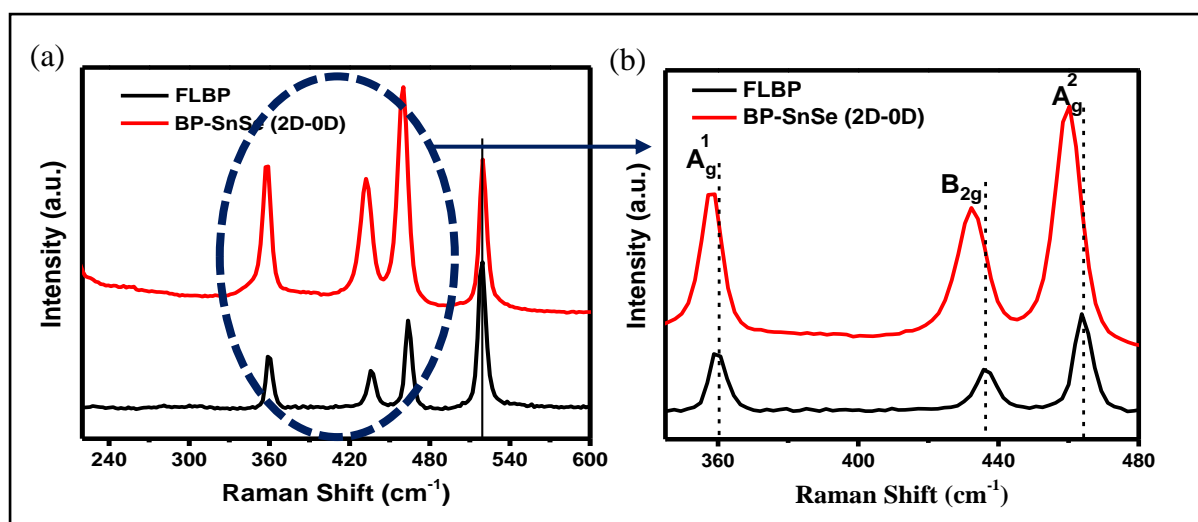

Figure 15: (a) Raman spectra of FLBP-SnSe NPs (red line) and FLBP (black line) (b) Enlarged Raman data, which clearly shows shift towards lower wavenumber. Shift in the Raman peaks allude to the interaction between BP sheets and SnSe NPs.

3.3.4. TEM

TEM images of FLBP-SnSe nanoparticles heterostructure are shown in Figure 16a, b. SnSe nanoparticles on BP sheets can be clearly seen in Figure 16b. HRTEM image (Figure 16c) shows SnSe NPs with (111) orientation on FLBP. Fringes seen in HRTEM were analysed using digital micrograph software from gutan. Fringe width of 0.16 nm indicates the distance between two P atoms in top-down view of puckered BP along x-axis.[29] In SAED pattern (Figure 16d), bright spots confirms the crystalline FLBP (d = 0.14 nm), while small spots with continuous rings shows the polycrystalline nature of the SnSe NPs (d = 0.28 nm). To check the spatial distribution of the elements mapping was done with TEM (Figure 16 e and f).
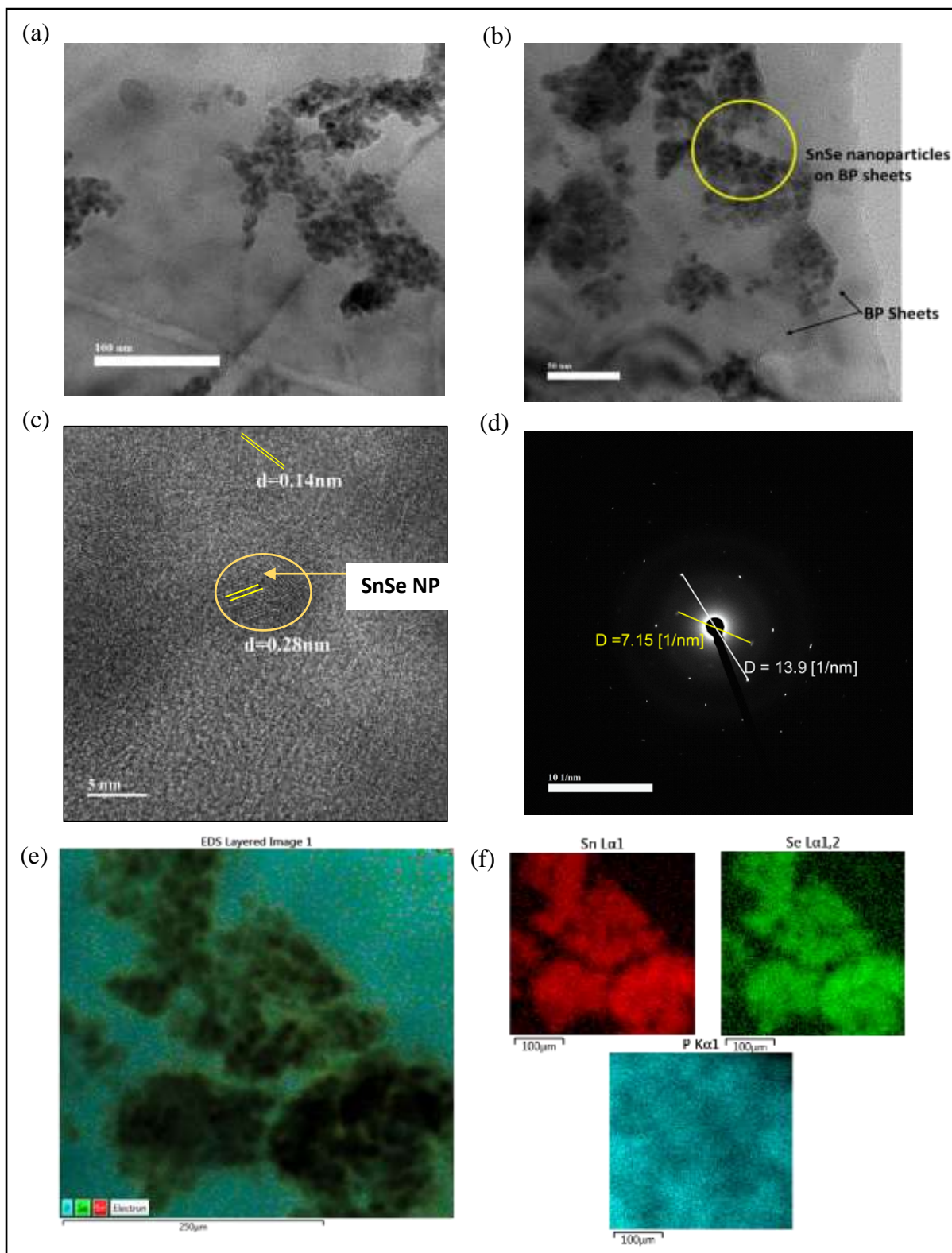
Figure 16: (a, b) TEM images of BP-SnSe (2D-0D) heterostructure on Cu grid coated with ultra-thin amorphous carbon (c) HRTEM image depicting (111)-oriented SnSe nanoparticle on BP sheet. (d) SAED pattern of the BP-SnSe heterostructure analysed using CrysTbox software. Bright spots in the SAED pattern corresponds to the crystalline FLBP while small dots with continuous rings corresponds to polycrystalline SnSe nanoparticles. (e, f) Elemental mapping by using TEM EELS

3.3.5. Photocurrent measurements

.

Figure 17: (a) Optical microscope image of the device with 50x lens showing the channel length (100µm). (b, c, d) SnSe NPs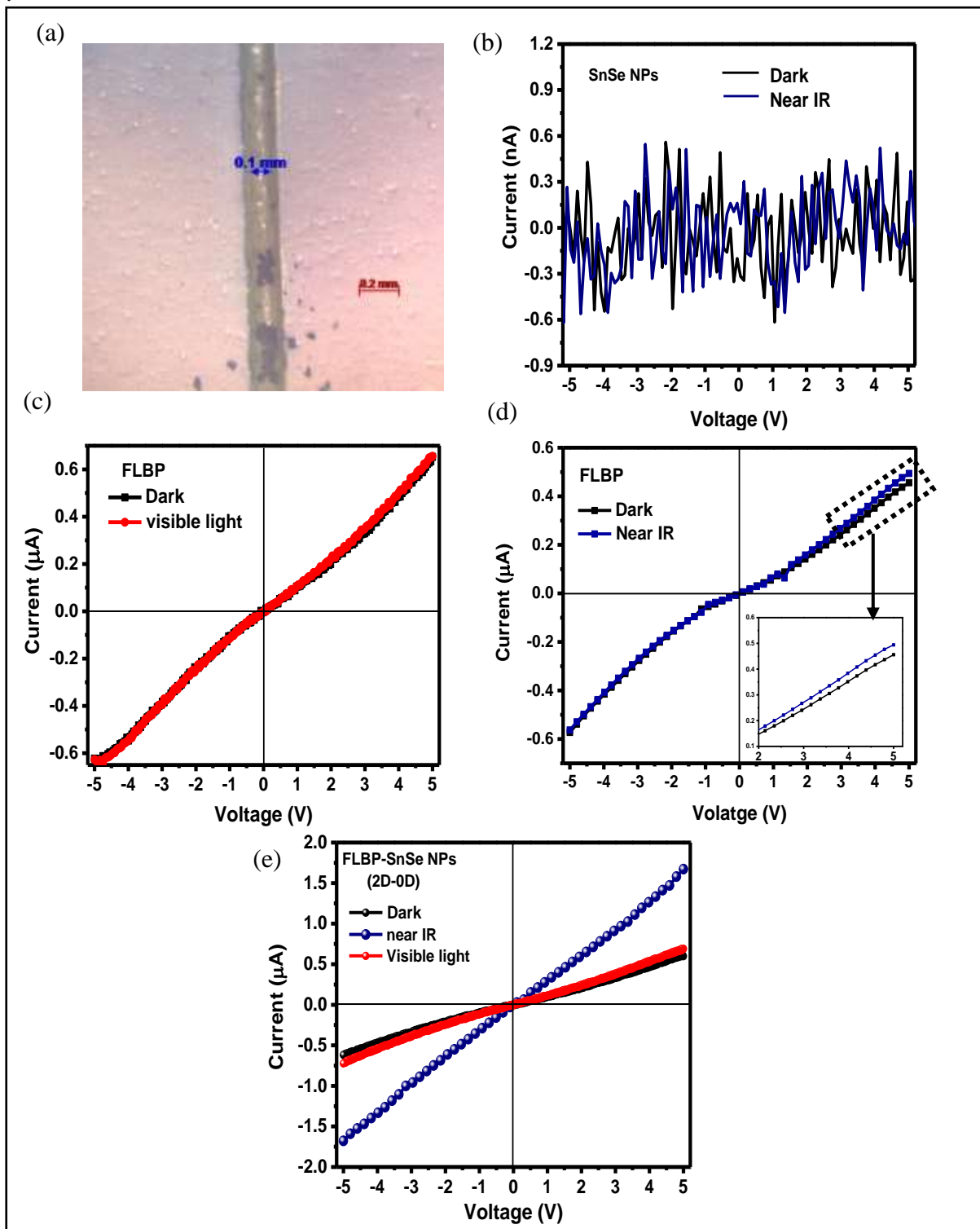 and FLBP in the dark and under illumination. (e) I-V characteristics of FLBP-SnSe (2D-0D) heterostructure in the dark (black line), under visible light illumination (red line) and NIR light illumination (blue line).

Optical microscope image and I-V characteristics of the prepared device are shown in Figure 17. Optical microscope image (analysed using ImageJ software) depicted the channel length of 100□m (Figure 17a). Dark current and NIR photocurrent recorded for SnSe nanoparticles were in nA range. In Figure 17b, I-V characteristics of the measured NIR photocurrent and dark current of SnSe NPs device are shown. As SnSe absorbs in IR and NIR regions, we can't expect any change in the visible light photocurrent. We have already discussed I-V characteristics of the FLBP in section 3.1.5. FLBP showed very small change in the current under illumination with NIR light. In case of FLBP-SnSe (2D-0D) heterostructure, there is considerable change in the current under NIR illumination. This change in the current can't be just because of thermoelectric effect due to IR radiation because, if this would have been the case then we could have seen considerable change in the current of FLBP and SnSe NPs too.

3.4. BP-Organic molecules Heterostructure:

3.4.1. UV-Vis Spectroscopy

Qualitative analysis of the prepared samples was done using Shimadzu UV 3600 with Quartz cuvette (1 cm pathlength). In absorption data, it was observed that all the organic molecules absorb only in the UV region. Moreover, they show excitonic peak at around 257 nm. While heterostructures of these molecules with FLBP shows sharp and strong excitonic peak at around 260 nm and absorb throughout UV-Vis-NIR region. So, there is small shift and enhancement in the excitonic peak of absorption spectrum of the heterostructures, which can be distinctly seen in Figure 18. In case of heterostructure, both scattering and absorption have contributed to the absorption spectra, and scattering is mainly because of BP sheets.
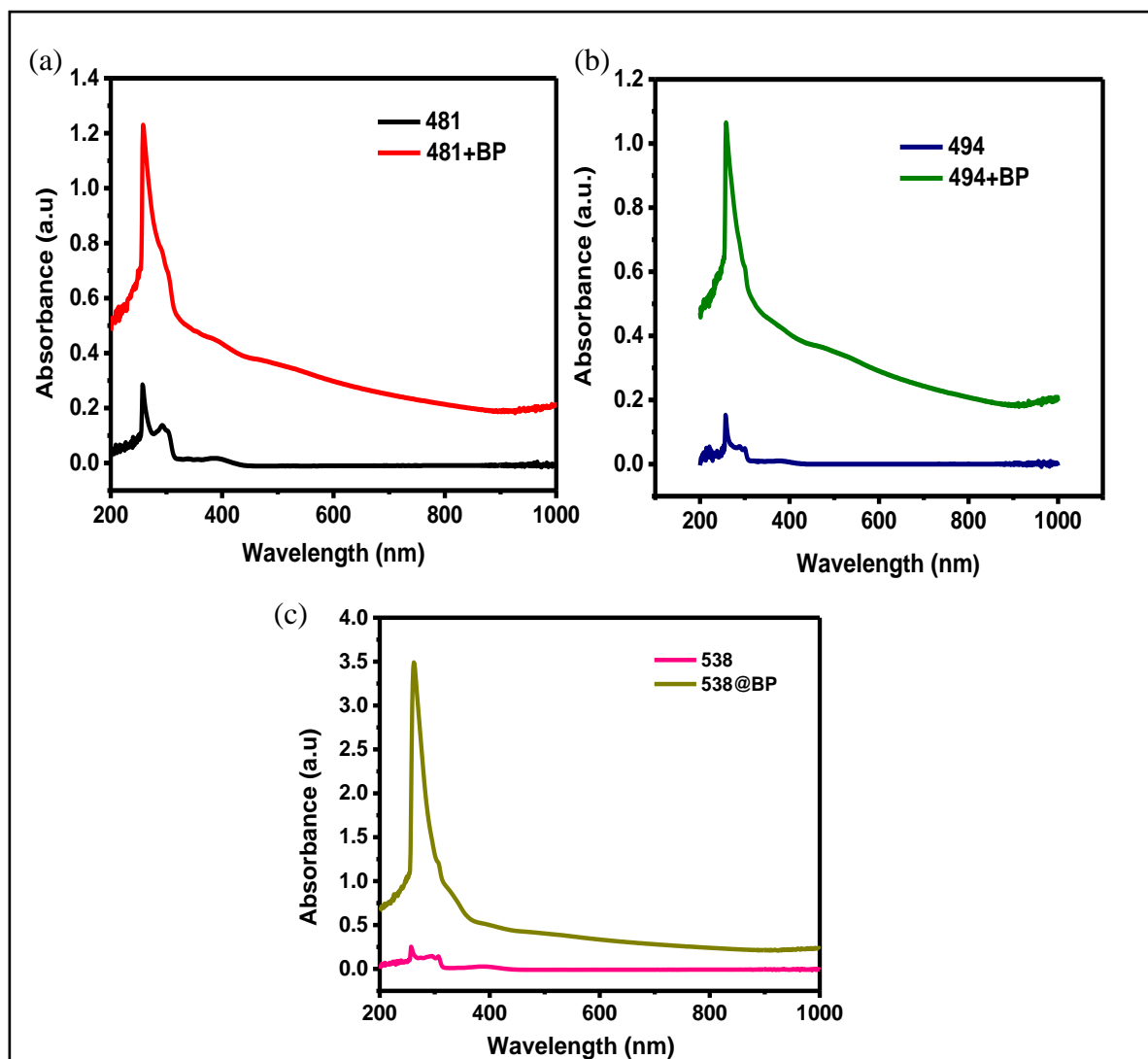
Figure 18: UV-visible absorption spectra of (a) CH-481 and CH-481+FLBP (b) CH-494 and CH-494+FLBP (c)CH-538 and CH-538+FLBP

3.4.2. Photoluminescence Spectroscopy

Photoluminescence (PL) and time resolved Photoluminescence were measured using FLS 980 (Edinburgh Instruments). PL spectra of the samples were taken to study the effect of addition FLBP at fixed concentration. PL spectra of the 481,494 and 538 molecules showed band-edge emission in the range of 400 nm to 650 nm with maxima at around 494.6 nm, 499 nm and 580 nm respectively. It was observed that the PL intensity was quenched on addition of FLBP (Figure 19a, b and c), which relates to the phenomenon of charge transfer from Aristolactum molecules to FLBP. This was further confirmed using time resolved photoluminescence (TRPL) where the time constants reduced in case of sample with FLBP in the range of 0.5 to 2.1 ns depending on the functional group of Aristolactum molecules.
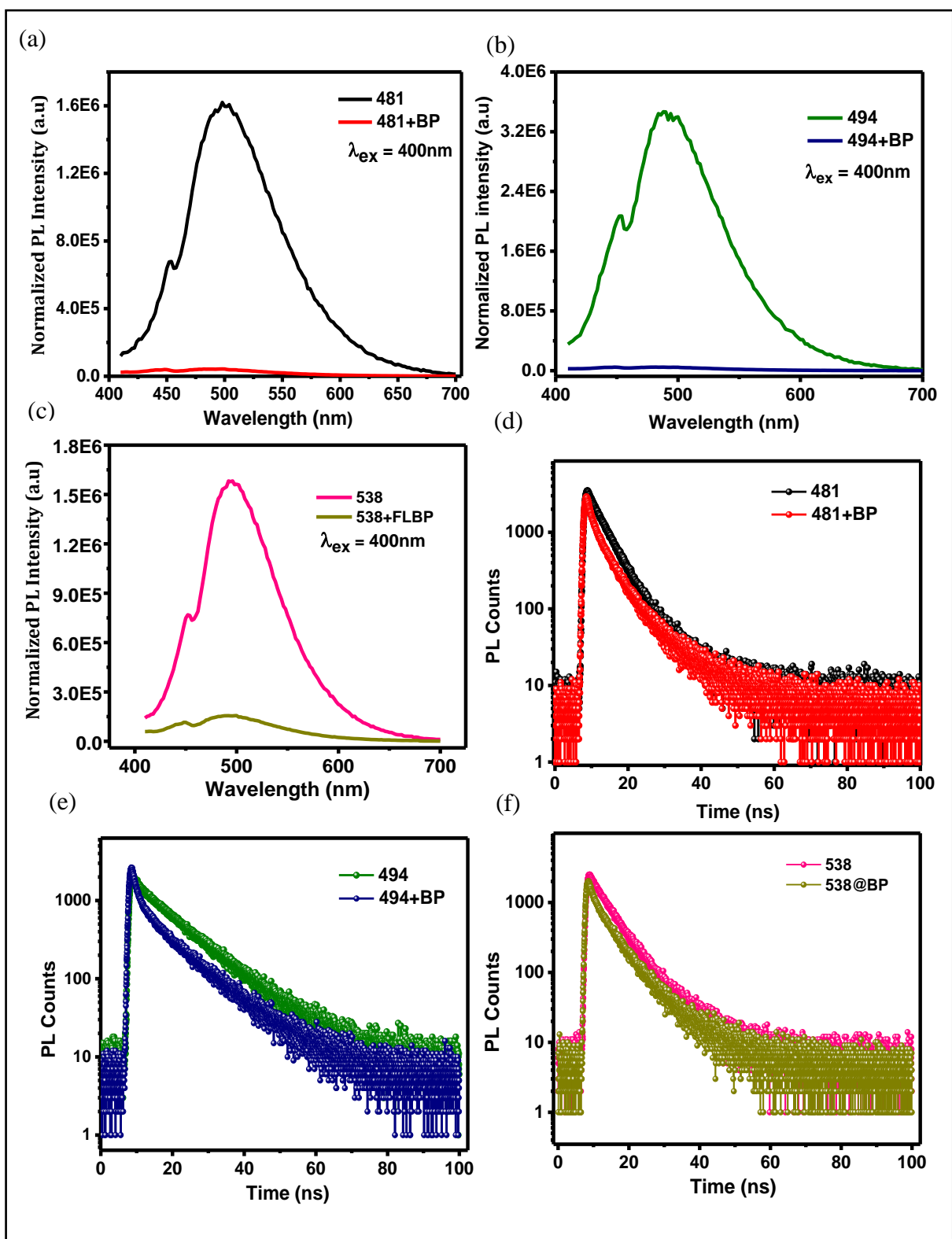
Figure 19: PL and TRPL spectra of CH-481, CH-481+FLBP, CH-494, CH-494+FLBP, CH-538 and CH-538+FLBP

Sample	494	494+BP	481	481+BP	538	538+BP
τ_1 (ns)	2.2	1.5	4.3	2.2	4.9	2.6
τ_2 (ns)	11.6	10.9	12.3	7.6	12.1	7.9
α_1	448.9	1848.6	3212	2073.4	2231.6	1218.3
α_2	1607.8	894.4	170.8	754.5	213.2	686.8
τ_{avg}(ns)	11.1	8.8	5.4	5.2	6.3	6
χ^2	1.08	1.24	1.15	1.49	1.2	1.38

3.4.3. Photocurrent Measurements:

BP absorbs over whole UV-Vis-NIR region but its absorption coefficient is low.[32] While organic molecules strongly absorbs in only UV range. So, we gave an attempt to make a heterostructure which can effectively absorbs in visible region. To check the application of the heterostructure as a photodetector, we prepared primitive devices with suitable organic molecules and checked its photo-response. The BP-organic molecules heterostructure showed good response under 405 nm laser (<50mW) illumination. Figure 20b and d shows I-V characteristics of the recorded dark current and visible-light photocurrent for FLBP-organic molecules heterostructures. Enhancement in the current under illumination can be distinctly seen in both cases. In Figure 20a and c, we can see that FLBP and Organic molecules doesn't show any change in the current under illumination. Organic molecules based devices have current in pA range. Because of sensitivity limitations we got noisy data in these cases. Time-resolved current was measured at constant bias of 1V with a LED source (9 mW) to get better idea about photo-response (Figure 20e and f). In this study, increase (decrease) in the current was observed when the light source was switched ON (OFF) and reaches a saturation. Moreover, upon illumination current increased every time on switching ON the light source. The possible reason for this might be that system was not in the steady state. We should have started the measurement after switching on the light source for some time.
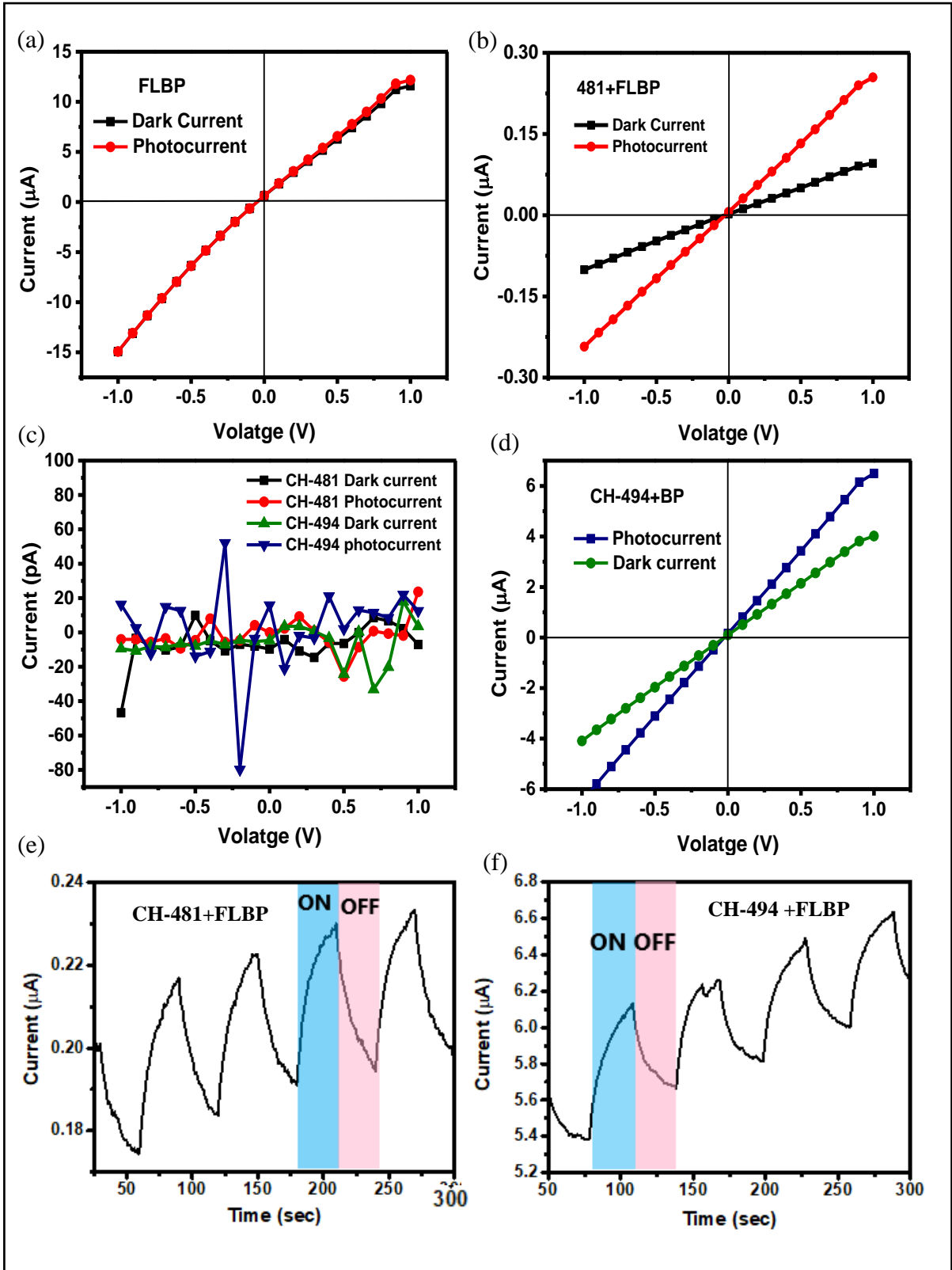
Figure 20: (a, b, c, d) I-V characteristics of measured dark current and photocurrent for FLBP, CH-481+FLBP, CH-481 and CH-494 molecules and CH-494+FLBP (e, f) Current-time curve of the CH-481+FLBP and CH-494+FLBP heterostructures devices.

4. Conclusion

We have explored 2D-2D and 2D-0D heterostructures of FLBP. The three heterostructures under study were: FLBP-SnSe (2D-2D), FLBP-SnSe NPs (2D-0D) and FLBP-organics molecules (2D-0D). These heterostructures were synthesised using solution processed techniques. XRD, TEM and Raman spectroscopy confirmed the formation of desired heterostructures. The FLBP-SnSe heterostructures were further probed in detail by Raman spectroscopy. Shift in the Raman peaks confirmed the interaction between BP and SnSe. To explore the applications of these heterostructures in optoelectronics, photovoltaic devices of all the three heterostructures were fabricated. Both the FLBP-SnSe heterostructures demonstrated the photo-response in the NIR region. Here, the FLBP-SnSe NPs heterostructure, was superior in performance as compared to the 2D-2D heterostructure. Moreover, the FLBP-Organic molecules heterostructure showed photoresponse under visible light illumination. This work will pave the way for the optoelectronic study of novel 2D-0D heterostructures.

Future Outlook

Spectral response of the FLBP-SnSe NPs heterostructure needs to be tested. To enhance the photovoltaic effects of the heterostructure, photodetectors has to be fabricated using photolithography/Electron beam lithography. In case of BP-SnSe heterostructures, as both BP and SnSe are highly anisotropic, the polarization sensitivity of the photodetector needs to be checked.

References

[1] E. Gazit, Plenty of Room for Biology at the Bottom: *An Introduction to Bionanotechnology*, Imperial College Press, London (2007)

[2] S. K. Sahoo, S. Parveen & J. J. Panda, *The present and future of nanotechnology in human health care*, Nanomedicine 3, 20 (2007).

[3] D. R. Boverhof et al. *Comparative assessment of nanomaterial definitions and safety evaluation considerations*, Regul. Toxicol. Pharmacol 73, 137 (2015).

[4] X. Zhang, L. Hou, A. Ciesielski, P Samori, *2D Materials beyond Graphene for High Performance Energy Storage Applications,* Adv. Energy Mater 6, 1600671 (2016)

[5] R. Mas-Ballesté, C. Gómez-Navarro, J. Gómez-Herrero & F. Zamora, 2D materials: to graphene and beyond, Nanoscale 3, 20 (2011)

[6] D. H. Cao, C. C. Stoumpos, O. K. Farha, J. T. Hupp & M. G Kanatzidis, *2D homologous perovskites as light-absorbing materials for solar cell applications*, J. Am. Chem. Soc. 137, 7843 (2015)

[7] T. Das, B.K. Sharma, A. K. Katiyar and Jong-Hyun Ahn, *Graphene-based flexible and wearable electronics*, J. Semicond. 39, 011007 (2018)

[8] W. H. Zhou, H. D. Cui, L. M. Ying, X. F. Yu, *Enhanced Cytosolic Delivery and Release of CRISPR/Cas9 by Black Phosphorus Nanosheets for Genome Editing*, Angew. Chem., Int. Ed. 57, 10268 (2018)

[9] S. Ahmed, J. Yi, *Two-Dimensional Transition Metal Dichalcogenides and Their Charge Carrier Mobilities in Field-Effect Transistors*, Nano-Micro Lett *9*, 50, (2017)

[10] Ming-Yang Li, Sheng-Kai Su, H.-S. Philip Wong & Lain-Jong Li, *How 2D semiconductors could extend Moore's law*, Nature 567, 169 (2019)

[11] Vy Tran, Ryan Soklaski, Yufeng Liang, and Li Yang, *Layer-controlled band gap and anisotropic excitons in few-layer black phosphorus*, Physical Review B 89, 235319 (2014).

[12] X. Zhang, L. Hou, A. Ciesielski, P. Samori, *2D Materials beyond Graphene for High Performance Energy Storage Applications,* Adv. Energy Mater 6, 1600671 (2016)

[13] S. Z. Butler, S. M Hollen, L. Cao, Y. Cui, J. A. Gupta, H. R. Gutiérrez et al., *Progress, Challenges, and Opportunities in Two-Dimensional Materials Beyond Graphene*, ACS Nano 7, 2898 (2013).

[14] R. W. Keyes, *The electrical properties of black phosphorus*, Phys. Rev. 92, 580 (1953)

[15] T. Hu & J. Dong, *Structural phase transitions of phosphorene induced by applied strains*, Physical Review B 92, 064114 (2015).

[16] P Chen, X. Chen, Ong, et at, *The Rising Star of 2D Black Phosphorus Beyond Graphene: Synthesis, Properties and Electronic Applications*, 2D Mater 5, 014002 (2018)

[17] W. Shi, M. Gao, J. Wei, J. Gao, C. Fan, E. Ashalley, H.Li, Z. Wang, *Tin selenide (SnSe): growth, properties, and applications,* Adv. Sci. 5, 1700602 (2018)
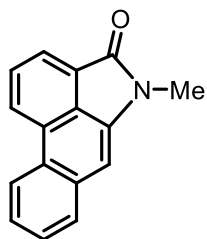
[18] G. Ding, G. Gao, & K. Yao, *High-efficient thermoelectric materials: the case of orthorhombic IV–VI compounds*, Sci. Rep. 5, 9567 (2015).

[19] L. D. Zhao, S. H. Lo, Y. S. Zhang, H. Sun, G. J. Tan, C. Uher, C. Wolverton, V. P. Dravid, M. G. Kanatzidis, *Ultralow thermal conductivity and high thermoelectric figure of merit in SnSe crystals*, Nature 508, 373 (2014)

[20] L. C. Gomes, A. Carvalho, *Phosphorene analogues: Isoelectronic two-dimensional group-IV monochalcogenides with orthorhombic structure*, Phys. Rev. B 92, 085406 (2015).

[21] X. B. Li et al. *Structures, stabilities, and electronic properties of defects in monolayer black phosphorus*, Sci. Rep. 5, 10848 (2015).

[22] L. Li et al. *Black phosphorus field-effect transistors*, Nat. Nanotech. 9, 372 (2014).

[23] L.-C. Zhang, G. Qin, W.-Z. Fang, H.-J. Cui, Q.-R. Zheng, Q.-B. Yan & G. Su, *Tinselenidene: a Two-dimensional Auxetic Material with Ultralow Lattice Thermal Conductivity and Ultrahigh Hole Mobility*, Sci. Rep. 6, 19830 (2016).

[24] Z. Luo et al. *Anisotropic in-plane thermal conductivity observed in few-layer black phosphorus*, Nat. Commun. 6, 8572 (2015).

[25] D. Jariwala, T. J. Marks & M. C. Hersam, *Mixed-dimensional van der Waals heterostructures*, Nat. Mater. 16, 170 (2017).

[26]   B. Pejjai, V. Reddy, M. Reddy, S. Gedi, C. Park, *Eco-friendly synthesis of SnSe nanopartricles: effect of reducing agents on the reactivity of a Se-precursor and phase formation of SnSe NPs*, New J. Chem. 42 (2018)

[27] S. Speakman, Estimating Crystallite Size Using XRD (MIT Center for Materials Science and Engineering, 2018)

[28] M. A. Franzman, C. W. Schlenker, M. E. Thompson, & R. L. Brutchey, *Solution-Phase Synthesis of SnSe Nanocrystals for Use in Solar Cells*, J. Am. Chem. Soc. 132, 4060 (2010).

[29] L. F. Gao, J. Y. Xu, Z. Y. Zhu, C. X. Hu, L. Zang, Q. Wang, H. L. Zang, *Small Molecule-Assisted Fabrication of Black Phosphorus Quantum Dots with a Broadband Nonlinear Optical Response*, Nanoscale 8, 15132 (2016)

[30] H. Tian, X.F. Wang, M.A. Mohammad et al. *A hardware markov chain algorithm realized in a single device for machine learning*, Nat Commun 9,4305 (2018)

[31] K. S. Novoselov, A. Mishchenko, A. Carvalho & A. H. Castro Neto, *2D materials and van der Waals heterostructures*, Science 353, aac9439 (2016).

[32] D. Hanlon et al. *Liquid exfoliation of solvent-stabilized few-layer black phosphorus for applications beyond electronics*. Nat. Commun. **6**, 8563 (2015).

[33] W. J. Yu et al. *Highly efficient gate-tunable photocurrent generation in vertical heterostructures of layered materials*. Nature Nanotech. 8, 952 (2013).

[34] L. Zhang, Q. Zeng, K. Wang, *Pressure-Induced Structural and Optical Properties of Inorganic Halide Perovskite $CsPbBr_3$*, J. Phys. Chem. Lett. 8, 3752 (2017).

[35] C. Chen, W.-H. Cheng, S.-S. Lin, *Study of Iron-Promoted Cu/SiO_2 Catalyst on High Temperature Reverse Water Gas Shift Reaction* Appl. Catal., A 257, 97 (2004).

[36] A. C. Ferrari, *Raman spectroscopy of graphene and graphite: Disorder, electron-phonon coupling, doping and nonadiabatic effects*, Solid State Comm. 143, 47 (2007).

[37] L. Viti, A. Politano and M. S. Vitiello, *Black phosphorus nanodevices at terahertz frequencies: Photodetectors and future challenges*, APL Materials 5, 035602 (2017).

[38] L. Li et al. *Direct observation of the layer-dependent electronic structure in phosphorene*, Nat. Nanotechnol. 12, 21(2017).

[39] W. Shi *et al.*, *Tin selenide (SnSe): growth, properties, and applications*, Adv. Sci. 5, 1700602 (2018).

[40] X.-H. Ma, K.-H. Cho, and Y.-M. Sung, *Growth mechanism of vertically aligned SnSe nanosheets via physical vapour deposition*, CrystEngComm 16, 5080 (2014).

[41] S. Speakman, *Estimating Crystallite Size Using XRD*, MIT Center for Materials Science and Engineering (2008).

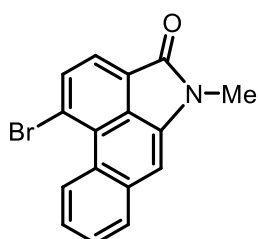[42] R. Jenkins and R. Snyder, *Introduction to X-ray Powder Diffractometry*, Wiley-Interscience (1996)

Appendix

Organic molecules used in this study are Aristolactum molecules. We got these molecules from Dr. Channa Reddy. Aristolactams are a minor group of fused phenanthrene lactam alkaloids. The richest source of this class of alkaloids is the family *Aristolochiaceae*.
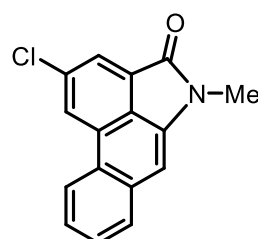
Molecular structure of the Aristolactum molecules used in the work are shown below:

CH-A-494   CH-A-481   CH-A-538